Springer

KSME

Journal of Mechanical Science and Technology 29 (1) (2015) 259~267
www.springerlink.com/content/1738-494x
DOI 10.1007/s12206-014-1232-x

Numerical and experimental investigations on the cavitation characteristics of a high-speed centrifugal pump with a splitter-blade inducer †

XiaoMei Guo[1], Linhang Zhu[2], ZuChao Zhu[3,*], BaoLing Cui[3] and Yi Li[3]

[1]*Zhejiang University of Water Resources and Electric Power, Hangzhou, 310018, China*
[2]*1201 Chu Kochen Honor College, Zhejiang University, Hangzhou, 310018, China*
[3]*The Zhejiang Provincial Key Laboratory of Fluid Transmission Technology, Zhejiang Sci-Tech University, Hangzhou, 310018, China*

(Manuscript Received July 23, 2014; Revised September 29, 2014; Accepted October 9, 2014)

Abstract

A high-speed centrifugal pump with a splitter-blade inducer is investigated in this work. The flow with rotating cavitation is numerically simulated, external characteristics are subjected to experimental tests, and the internal flow is visualized. These procedures are conducted to obtain the pressure, velocity, and vapor volume fraction distribution in the inducer and the impeller of the centrifugal pump. Bubble occurrence, development, and collapse are also observed. The predicted *H*-*Q* and η-*Q* curves agree with the experimental results of external characteristics. The calculated vapor volume fraction also agrees with the experimental results obtained from the visualization system. The mechanism of bubble evolution and the anti-cavitation performance of the high-speed centrifugal pump with a splitter-blade inducer are clearly elucidated.

Keywords: Centrifugal pump; External characteristics experiments; Rotating cavitation; Splitter-blade inducer; Visualization experiments

1. Introduction

Centrifugal pumps have been widely applied in different industries, including the petro-chemical, aerospace, and energy industries. With the rapid development of these industries, centrifugal pumps are required to increase in speed. In such cases, cavitation frequently occurs. Equipping an inducer in front of the main centrifugal impeller is an effective method to suppress cavitation [1]. A splitter-blade inducer is a common type and highly contributes to the anti-cavitation performance of pumps. The flow in the splitter-blade inducer is highly turbulent, particularly during cavitation. Several numerical and experimental studies have recently investigated the cavitating flow of a centrifugal pump with a forward-attached inducer. Li et al. [2] and Okita et al. [3] showed that the numerical simulation of the performance of a centrifugal pump with an inducer agrees with experiments conducted on test models. Semenov et al. [4] performed simulations and experiments on the cavitating flow in an inducer. They discovered a new type of cavitation instability in the pump. Pouffary et al. [5] simulated the cavitation behavior of a four-blade rocket engine turbo pump inducer and observed five cavitation patterns. Kim et al. [6] investigated the effects of tip clearance on the anti-cavitation performance and flow characteristics of a turbo pump inducer by using the computational fluid dynamics (CFD) approach. They found that cavitation is generated on the long blade for large tip clearances and that this cavitation obstructs the throat between two adjacent blades. Lee et al. [7] conducted experimental and numerical investigations on the cavitation instability of a two-bladed inducer. They found that the local flow around the cavity closure significantly contributes to the occurrence of asymmetric cavitation. Iga et al. [8] found three types of cavitation surges in an inducer on the basis of oscillation characteristics and flow fields. Campos-Amezcua et al. [9] numerically simulated an unsteady cavitating flow and explored local cavitation instabilities, such as alternate blade cavitation and rotating blade cavitation, which can appear in axial inducers. Tamura et al. [10] established a bubble dynamics model to improve simulation quality. Yoshida et al. [11] tested four-bladed inducers with various amounts of cutback to suppress rotating cavitation by applying alternate leading edge cutback. They showed that regions with alternate blade cavitation and asymmetric cavitation become enlarged with an increasing cutback amount. Yoshida et al. [12] investigated the relationship of the uneven cavity length and rotor dynamic force in a cavitating inducer with three blades. They indicated that the shaft vibration because of rotating cavitation is a type of self-excited vibration arising from the coupling of cavitation instability and rotor dynamics. Tani

*Corresponding author. Tel.: +86 13906507577, Fax.: +86 57185111686
E-mail address: zuczhu@163.com
† Recommended by Associate Editor Shin Hyung Rhee

et al. [13] investigated the relationship between the rotating cavitation and flow coefficient of an inducer through numerical simulations. They showed that the flow coefficient influences the onset of cavitation instabilities, such as rotating and asymmetric cavitation. Horiguchi et al. [14] analyzed steady cavitating flow in cascades and found that the stability of the flow affects the camber and blade thickness. Horiguchi et al. [15] found that the three-dimensionality of cavitating flow changes the angle of attack, which is associated with the change in meridional velocity. Kimura et al. [16] researched the vortex structure in the inducer for three types of inlet casing geometries with various flow rates. Their results showed that the development of the tip leakage vortex is dependent on the inlet casing geometry and the flow rate. Hong et al. [17] experimented on a pump with an inducer and found that the inducer exhibits a negligible effect on the head and efficiency of the pump but exerts a significant effect on anti-cavitation performance.

Many scholars [18-22] have focused on cavitation and arrived at certain conclusions. However, research on the anti-cavitation characteristics of a high-speed centrifugal pump with a splitter-blade inducer is insufficient. Moreover, the external characteristics and visualization of internal flow have been rarely experimented. Therefore, investigations on the rotating cavitation characteristics of a centrifugal pump with a splitter-blade inducer are essential.

This study aims to numerically and experimentally investigate the rotating cavitation characteristics of a high-speed centrifugal pump with a splitter-blade inducer. The objective of this work is to analyze the cavitation around the splitter-blade inducer and the impeller of the centrifugal pump. The rotating cavitation is numerically investigated with the use of a mixture model through the CFD approach. Experiments on the external characteristics of the centrifugal pump are performed on a closed system. The cavitating flow in the inducer is observed by visualization with a high-speed video system. The unsteady behavior of cavitation is discussed by comparison of the numerical results with the experimental data.

2. Numerical calculation of the rotating cavitation

A high-speed centrifugal pump with a splitter-blade inducer shown in Fig. 1 is used as the research object, whose design parameters and main dimensions are listed in Table 1. The final mesh along the inducer and the impeller is shown in Fig. 2. For the complex 3D geometry of blades, unstructured grids are utilized in the simulation. The grid number of the entire centrifugal pump with the splitter-blade inducer is 93, 3109. The 3D turbulent cavitating flow is solved with the use of unsteady Navier-Stokes equations, coupled with the Reynolds average simulation approach and a mass transfer cavitation model. The commercial software ANSYS-CFX is used for the simulation.

The boundary conditions are set as follows:

The inlet pressure is specified at the inlet. In this sample, the total pressure is set as 15,590 Pa. The mass flow rate is specified at the outlet, and it is set as 0.875 m/s. These values are obtained through experiments on external characteristics. For the two-phase flow, a mixture model is used [23-25]. Two phases are considered as water and vapor [2, 26, 27]. The water temperature is assumed as 25°C during the simulation, which indicates that the saturated steam pressure is 3167 Pa.

Table 1. Main design parameters and dimensions of the high-speed centrifugal pump.

Main design parameters			
Flow rate Q (m^3/h)	Head H (m)	Rotation speed n (r/min)	Specific speed n_s(n_s=3.65×n×$Q^{0.5}$/$H^{0.75}$)
4	100	6000	23.08

Main dimensions			
Inlet diameter, D_1	40 mm	Number of blades of the impeller Z_I	8
Outlet diameter, D_2	40 mm	Height from the centerline of the inlet to the outlet, Z	196 mm

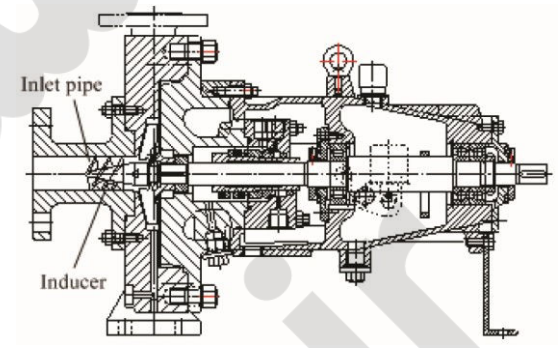

(a) Pump with a splitter-blade inducer

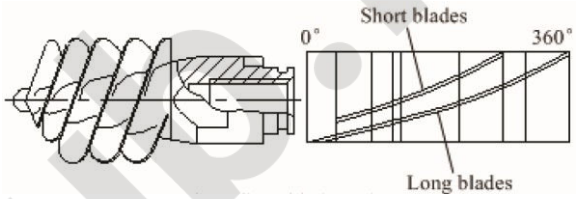

(b) Splitter-blade inducer

Fig. 1. Centrifugal pump with a splitter-blade inducer.

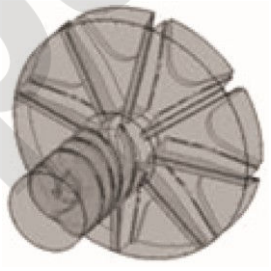

(a) Passage of the inducer and impeller

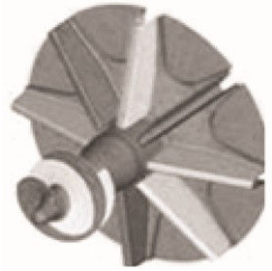

(b) Grids along the inducer and impeller

Fig. 2. Computational grids on the rotating parts.

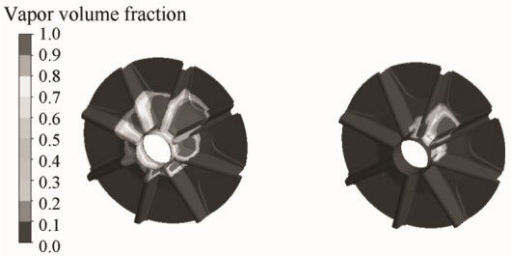

(a) Without an inducer (b) With a splitter-blade inducer

Fig. 3. Vapor volume fraction distribution on the impeller.

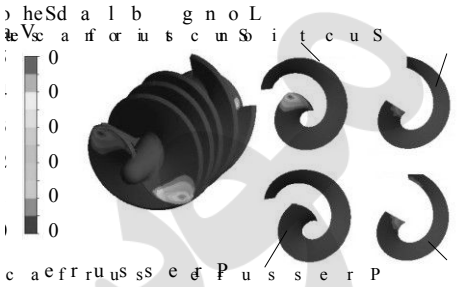

Fig. 4. Vapor volume fraction distribution on the splitter-blade inducer.

To accelerate the speed of convergence, calculation is repeated until it converges under single-phase steady flow. Then, the result is considered as the initial flow of the two-phase unsteady flow.

During simulation, a physical model is based on the assumption that the mixture of water and vapor in a cavitating flow is regarded as a homogeneous fluid. The Reynolds average simulation approach is used in this study. A mixture model is used, and the number of phases is set as two. The two phases are considered as water-liquid and water-vapor. The continuity of mass and the momentum are expressed as

$$\frac{\partial \rho}{\partial t}+\frac{\partial}{\partial x_j}\left(\rho u_j\right)=0 \tag{1}$$

$$\frac{\partial}{\partial t}\left(\rho u_i\right)+\frac{\partial}{\partial x_j}\left(\rho u_i u_j\right)=-\frac{\partial P}{\partial x_i}+\frac{\partial}{\partial x_j}\left(\mu \frac{\partial u_i}{\partial x_j}\right), \tag{2}$$

for which

$$\rho=\alpha_w \rho_w+\alpha_v \rho_v . \tag{3}$$

The volume fraction equation for the vapor phase is

$$\frac{\partial}{\partial t}\left(a_v \rho_v\right)+\nabla \cdot\left(a_v \rho_v \vec{v}_m\right)=-\nabla \cdot\left(a_v \rho_v \vec{v}_{dr,v}\right). \tag{4}$$

No slip boundary condition is specified at the wall. The moving coordinate system is used in the passage of the inducer and the impeller, with a rotation speed of 6000 r/min, whereas the static coordinate system is employed in the passage of the inlet pipe and the volute.

Flow calculations of the pump without and with a splitter-blade inducer are conducted. The calculated vapor volume fraction distributions on the impeller without and with a splitter-blade inducer are shown in Fig. 3.

Fig. 3(a) shows that the vapor volume fraction distribution in the impeller is concentrated and wide. Each passage contains many bubbles, filling almost three-quarters of the impeller passage. The observed cavitation is highly severe. The cavitation area is approximately 2,827 mm^2. Therefore, the anti-cavitation performance of the high-speed centrifugal pump without an inducer is very poor. Fig. 3(b) shows that the vapor volume fraction is obviously reduced when the pump has a splitter-blade inducer. The bubbles only occur in one passage, and the bubbles on the suction surface of the blades are more than those on the pressure surface. The cavitation area is approximately 314 mm^2. Therefore, the anti-cavitation performance of the centrifugal pump can be significantly improved with the use of a splitter-blade inducer.

The vapor volume fraction distribution on the splitter-blade inducer is shown in Fig. 4. The cavitation is focused on the suction surface of the long blades. The location of the cavitation is mainly on the outer edge near the blade inlet, where the vapor volume fraction is large. The distribution on the two long blades is asymmetric. The cavitation area on long blade 1 is approximately 69 mm^2, whereas that on long blade 2 is approximately 58 mm^2. The hub side near the blade outlet is also observed to cavitate. It may be affected by posterior low pressure. Almost no bubble can be found on the pressure surface of the blades. The vapor volume fraction on the short blades is only 1.25×10^{-6}, which is negligible.

To define the development of cavitation, the rotating cavitating flow of the high-speed centrifugal pump with the inducer is numerically calculated under different cavitation coefficients. Figs. 5 and 6, respectively show the vapor volume fraction distributions on both the impeller and the inducer under different cavitation coefficients.

From Fig. 5, we can conclude that the cavitation development on the impeller can be divided into three stages with the decline of the cavitation coefficient. The three stages are as follows.

Stage 1: Slow development stage

When the cavitation coefficient ranges from 0.1 to 0.07, the cavitation area is mainly on the suction surface of passage 1 of the blade. The area of the cavitation is small, and it slowly develops from 38 mm^2 to 97 mm^2. At this stage, the cavitation development speed is very slow.

Stage 2: Rapid growth stage

When the cavitation coefficient ranges from 0.06 to 0.02, the cavitation on the impeller rapidly grows. The location extends to both sides of passage 1. The area develops from approximately 241 mm^2 to 1216 mm^2. In this stage, the cavitation rapidly grows.

Stage 3: Backward extension stage

When the cavitation coefficient is from 0.04 to 0.02, the cav-

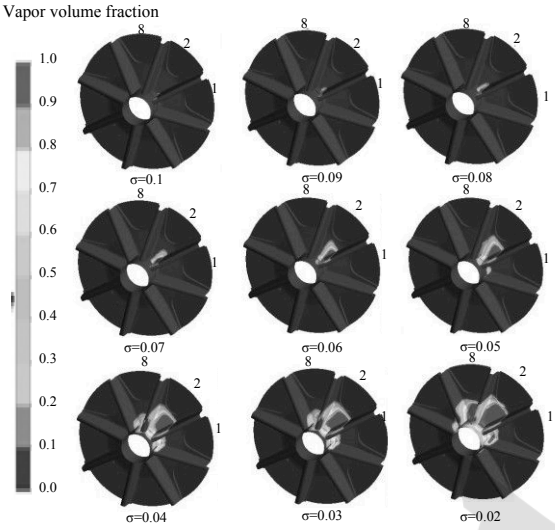

Fig. 5. Vapor volume fraction distribution on the impeller under different cavitation coefficients.

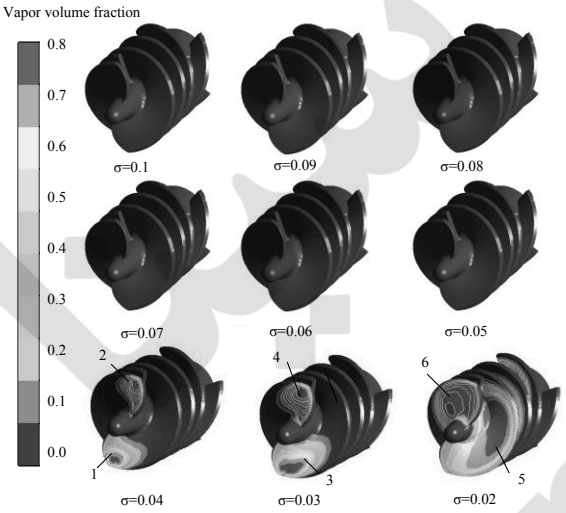

Fig. 6. Vapor volume fraction distribution on the inducer under different cavitation coefficients.

itation mainly develops in passage 8. It also develops in passage 2, but not so much as in passage 8. This result is related to the rotating direction. In this sample, the rotation is clockwise, so it is mainly backward extension (passage 8). This stage and the second stage overlap.

Fig. 6 shows that the vapor volume fraction gradually increases with the decrease in the cavitation coefficient. When σ ranges from 0.1 to 0.05, the vapor volume fraction in the inducer is rare, and its ratio is only approximately 2.384×10^{-7}. When σ is 0.04 and 0.03, the cavitation region is mainly located on areas 1, 2, 3, and 4, which are all on the outer edge of the suction surface near the inlet. The cavitation area is approximately 338 and 367 mm^2. When σ is 0.02, inducer cavitation covers a large area (about 1000 mm^2), and the location also varies. The cavitation location offsets to the outlet direction of the blades and hub side (see regions 5 and 6). The area where the cavitation occurs is asymmetric. When σ is 0.04, the area difference between regions 1 and 2 is approximately 21 mm^2. When σ is 0.03, the area difference between regions 3 and 4 is approximately 31 mm^2. When σ is 0.02, the area difference between regions 5 and 6 is approximately 85 mm^2. Therefore, the asymmetry becomes serious with a decrease in cavitation coefficient.

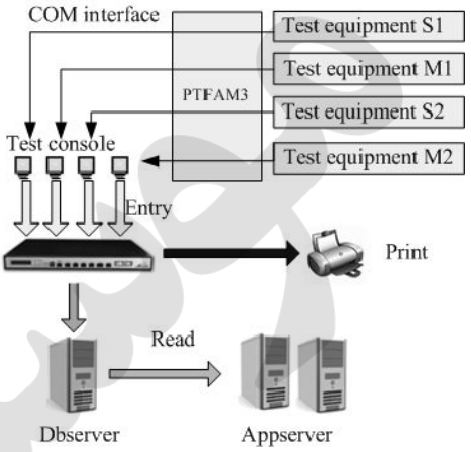

Fig. 7. DCS distribution.

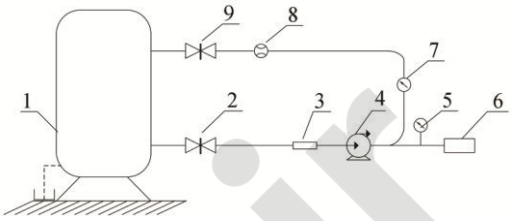

1. Circulation water tank
2. Valve
3. Water regulator section
4. High-speed centrifugal pump
5. Torque meter
6. Progressive frequency motor
7. Pressure meter
8. Turbine flowmeter
9. Electronic control valve

Fig. 8. Experiment set-up on external characteristics.

3. Experiments on external characteristics

The experimental set-up is shown in Fig. 7. A distributed control system (DCS) is used, and its distribution is shown in Fig. 8. The high centrifugal pump with a splitter-blade inducer is assembled on the closed system. The volume of the circulated water tank is 31 m^3. The vacuum pump is connected to the system. Its vacuity is up to 6×10^{-2} Pa. A type-NJ1G rotation torque meter is utilized to measure the rotation speed and shaft power. The allowable rotation speed ranges from 0 r/min to 10,000 r/min. The motor, sensor, and pump must be assembled in good concentricity.

The external characteristic curves are obtained through experiments and simulations (Fig. 9). The equations of head and efficiency are listed as follows.

Table 2. Inlet pressure value when the head suddenly decreases.

Inlet pressure value (Pa) $Q = 2$ m^3/h			Inlet pressure value (Pa) $Q = 4$ m^3/h		
By simulation	By experiment	relative error	By simulation	By experiment	Relative error
−96314	−92206	4.42%	−101085	−95245	3.91%

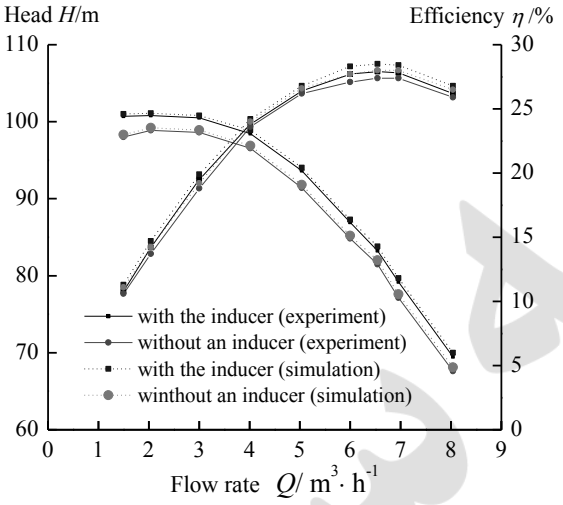

Fig. 9. External characteristic curves.

$$H = \Delta P/\rho g + \Delta z \tag{5}$$

$$\eta = \frac{nM}{9552\rho gQH} \times 100\% . \tag{6}$$

Fig. 9 shows that the characteristic curves obtained in the experiments are consistent with the curves obtained in the simulations. On the same flow rate (Q), the head (H) of the high-speed centrifugal pump with the splitter-blade inducer is higher than that without the inducer. The head value obtained in the simulation is also higher than that obtained in the experiment, and the largest difference is approximately 0.5 m. The trends of the η -Q curves obtained in the experiment and simulation are also similar. The efficiency value obtained in the numerical calculation is higher than that obtained in the experiment. The relative error is 2.3%. The main reason for this difference is losses, such as line loss. However, the losses can be neglected in the numerical calculation. This error can be considered a system error in forecasting the performance of the high-speed centrifugal pump.

Table 2 shows the inlet pressure when the head suddenly decreases. The difference between the simulation and experimental results is minimal. On the flow rate Q = 2 m^3/h, the relative error is approximately 4.42%. On the design flow rate Q = 4 m^3/h, the relative error is approximately 4%.

Fig. 10 shows the $NPSH_r$ value. Basing on Fig. 10, we can draw the following conclusions:

The $NPSH_r$ of the pump without the inducer is larger than that of the pump with the inducer, whenever it is used on the design work conditions regardless of the flow rate. This result indicates that the pump without an inducer has poor anti-cavitation performance. The $NPSH_r$ of the pump decreases when a splitter-blade inducer is positioned in front of the impeller. This finding suggests that the pump with an inducer has good anti-cavitation performance.

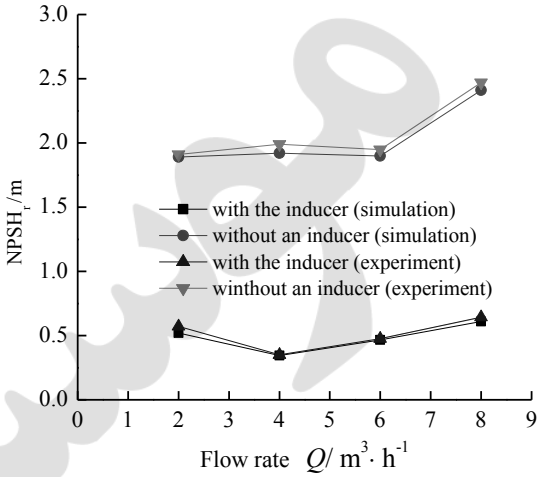

Fig. 10. $NPSH_r$ versus flow rate.

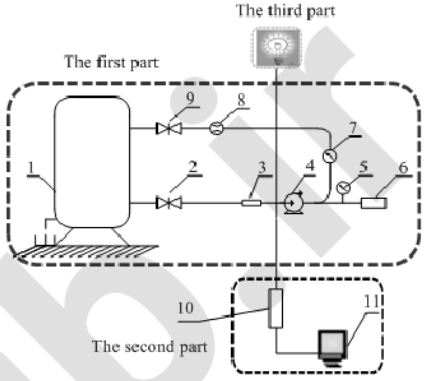

Fig. 11. Visualization experimental system.

The comparison between the simulations and the experiments demonstrates that the value of $NPSH_r$ obtained in the simulation is very nearly and only slightly lower than that obtained in the experiment.

4. Visualization system

The visualization experimental set-up is shown in Fig. 11, which includes three parts: closed experimental system (Fig. 8), high-speed camera system, and illumination part. The PCO.1200 hs high-speed camera developed by American Cooke Company is used in this sample.

To observe the cavitation and evolution, the pump body is designed into two parts, namely, (I) import and (II) main, as shown in Fig. 12. The import part is transparent and manufac-

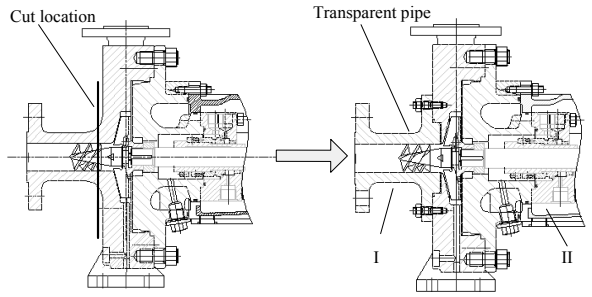

Fig. 12. Import pipe.

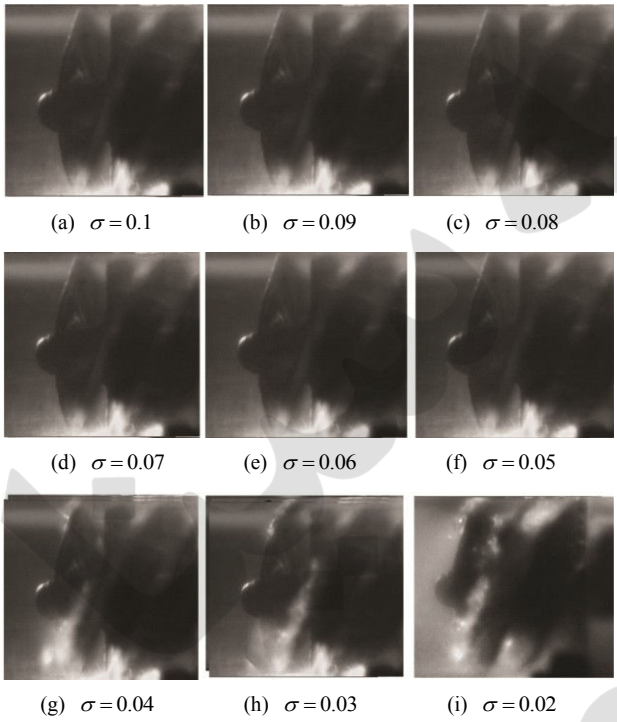

Fig. 13. Bubble development.

tured with organic glass. To allow the camera to focus well, a transparent rectangular sleeve is manufactured outside the import circle pipe. During the experiment, the rectangular sleeve should be filled with water. When the experiment is conducted, the effect of refraction will be compensated for.

The cavitation coefficient σ ranges from 0.1 to 0.02. The images of bubble development under different cavitation coefficients are captured with the use of a high-speed camera (Fig. 13).

The numerical calculation reflects the vapor volume fraction and cavitation location, among other aspects. The quantization effect is obvious, but it cannot directly observe the size, shape, and development of the bubbles. The visualization system must be highly intuitive to observe the occurrence, development, and collapse of the bubbles. Comparing Fig. 6 with Fig. 13, we can observe that the experimental data agree with the numerical results.

When σ ranges from 0.1 to 0.05, the bubbles in the inducer

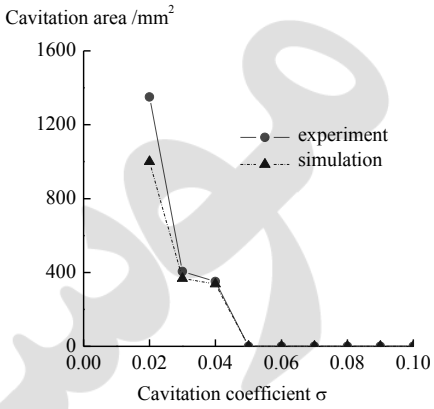

Fig. 14. Cavitation area and σ curves obtained in the simulation and experiment.

are very small, almost non-existent (Fig. 13). When σ ranges from 0.04 to 0.03, the bubbles can be easily observed. The cavitation region is mainly located on the suction surface of the blade where the outside edge is near the inlet. According to the outside measurement and estimation, the diameter of the formed bubbles ranges from 2 mm to 2.5 mm, and the coverage of the bubbles is approximately 350 and 400 mm^2. When σ is reduced to 0.02, the cavitation location simultaneously offsets to the outlet of the blade and to the hub side. Many bubbles fill the passages, and the area is approximately 1350 mm^2. Fig. 14 shows the cavitation area and σ curves determined in the simulations and experiments, which indicate that the simulation results agree with the experimental ones.

Therefore, the numerical calculation and visualization experimental results are consistent, and they can be divided into three stages as follows:

Stage 1: Cavitation inception stage in the inducer

When the cavitation coefficient σ ranges from 0.1 to 0.05, the bubble formation in the inducer is nearly not visible, and it can almost be neglected. The high-speed camera can be used to capture the micro-bubbles under these cavitation coefficients. The results show that the bubbles are on the outside of the suction surface near the inlet. From their generation to collapse, the bubbles show an irregular shape, and the time interval between these two processes is very short. The results are consistent with the simulations, as shown in Fig. 6 and can also be seen in Fig. 14.

The cavitation inception stage in the inducer is shown in Fig. 15. The bubble is generated with a nearly circular shape and a diameter of approximately 0.6 mm. Then, the diameter rapidly increases, and the shape becomes irregular. The bubble tends to split into two, and the total area becomes about twice of the original. After 0.4 ms, the bubble is divided into two parts. After another 0.4 ms, the two parts gradually become small until they completely collapse and disappear in the subsequent 2.0 ms or so.

Stage 2: Development stage

When the cavitation coefficient σ ranges from 0.04 to 0.03,

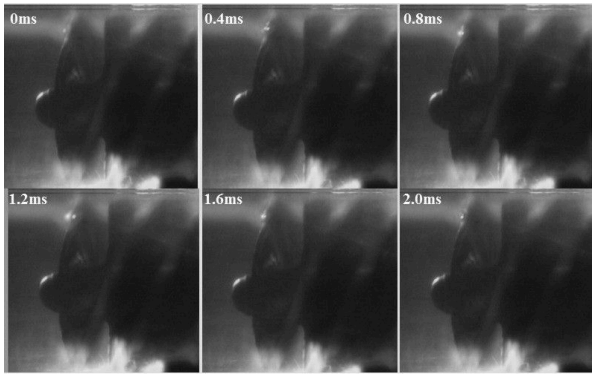

Fig. 15. Cavitation inception stage in the inducer passages.

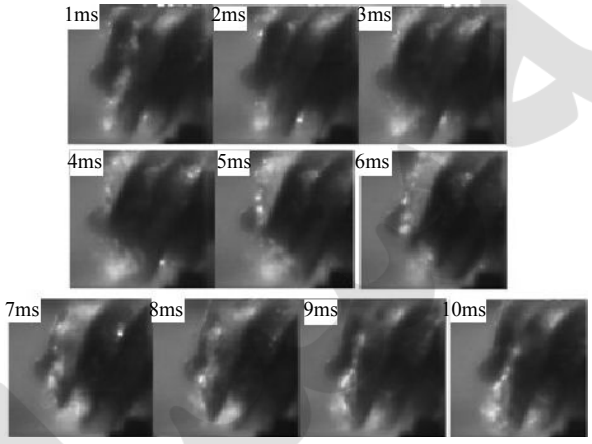

Fig. 16. Bubbles in the inducer passages as the pump rotates one revolution.

the cavitation position and bubble group formation are basically stable, and bubble grouping always exists. According to the numerical results, many bubbles appear under the cavitation coefficient range of 0.04 to 0.03, and the cavitation region is mainly located on the edge of the suction surface inlet. The region is asymmetric, and the asymmetry strengthens with a decrease in the cavitation coefficient.

Stage 3: Degradation stage

When the cavitation σ is 0.02, the performance of the pump rapidly declines with the occurrence of cavitation. The bubbles in the inducer passages as the pump rotates one revolution are shown in Fig. 16.

Fig. 16 shows 10 ms in 1 ms intervals, and the time is just a single revolution of the pump. The shape and the degradation stage of the bubbles can be clearly observed. The bubbles form at the outer edge of the suction surface of the long blades. Some bubbles also appear on the suction surface of the short blades. With the rotation of the inducer, bubbles follow the blade rotation. Under centrifugal force, the bubbles are thrown to the transparent pipe wall. During the experiment, the vibration and noise become obvious. The bubbles near the suction surface are so large that they are close to the pressure surface of the next blade. During the entire movement, the shape of the bubbles is disorderly and unsystematic. The bubbles in the blade passages produce a "jam" effect, which rapidly decreases pump performance.

5. Conclusions

The rotating cavitation characteristics of a high-speed centrifugal pump with a splitter-blade inducer are investigated through numerical simulation, external characteristics, and a visualization system. The following conclusions can be drawn.

A methodology that includes a cavitation model based on the Rayleigh-Plesset equation and a mixture model can be used to simulate the rotating cavitating flow of a centrifugal pump with a splitter-blade inducer. The numerical results agree with the experimental observation.

The simulations and experiments show that the cavitation development on the impeller can be divided into three stages with a decrease in cavitation coefficient. These stages are slow development, rapid growth, and backward extension.

The cavitation development on the splitter-blade inducer can be divided into three stages, namely, cavitation inception, development, and degradation.

Furthermore, the relationship of the inducer and the cavitation degree of the main impeller is demonstrated. The asymmetry becomes serious with a decrease in cavitation coefficient.

Acknowledgment

This work is financially supported by the National Natural Science Foundation of China (Project Nos. 51406185 and 51276172), the China Scholarship Council Project in 2012 (No. 201208330325), the Third Level 151 Talent Project in Zhejiang Province, and the Professional Leader Leading Project in 2013 (No. lj2013005).

Nomenclature

H : Head, m
N : Rotation speed, r/min
n_s : Specific speed
Q : Flow rate, m^3/h
η : Efficiency, %
$NPSH_r$: Net positive suction head must, m
P_{in} : Inlet pressure, Pa
ρ : Mixture density, kg/m^3
α_w : Volume fraction of liquid phase
α_v : Volume fraction of vapor phase
u : Mixture mass average velocity, m/s
ρ_w : Density of liquid phase, kg/m^3
ρ_v : Density of vapor phase, kg/m^3
u_w : Velocity of liquid phase, m/s
u_v : Velocity of vapor phase, m/s
P : Pressure, Pa

ΔP : Pressure difference between outlet pressure and inlet pressure, Pa

Δz : Vertical distance between impeller center and pump outlet, m

M : Torque, N·m

References

[1] Y. D. Choi, J. Kurokawa and H. Imamura, Suppression of cavitation in inducers by j-grooves, *ASME J. Fluids Eng.,* 129 (1) (2007) 15-22.

[2] Y.j. Li and F.j. Wang, Numerical investigation of performance of an axial-flow pump with inducer, *Journal of hydrodynamics*, 19 (6) (2007) 705-711.

[3] K. Okita, H. Ugajin and Y. Matsumoto, Numerical analysis of the influence of the tip clearance flows on the unsteady cavitating flows in a three dimensional inducer, *Journal of Hydrodynamics*, 21 (1) (2009) 34-40.

[4] Y. A. Semenov, A. Fujii and Y. Tsujimoto, Rotating choke in cavitating turbo-pump inducer, *ASME J. Fluids Eng.,* 126 (1) (2004) 87-93.

[5] B. Pouffary, R. F. Patella, J. L. Reboud and P. A. Lambert, Numerical analysis of cavitation instabilities in inducer blade cascade, *ASME J. Fluids Eng*., 130 (4) (2008) 041302.

[6] S. Kim, C. Choi, J. Kim, J. Park and J. Baek, Tip clearance effects on cavitation evolution and head breakdown in turbopump inducer, *Journal of Propulsion and Power*, 29 (6) (2013) 1357-1366.

[7] K. Lee, J. Choi and S. Kang, Cavitation performance and instability of a two-bladed inducer, *Journal of Propulsion and Power*, 28 (6) (2012) 1168-1175.

[8] Y. Iga, K. Hashizume and Y. Yoshida, Numerical analysis of three types of cavitation surge in cascade, *ASME J. Fluids Eng.*, 133 (7) (2011) 071102.

[9] R. Campos-Amezcua, S. Kehelladi, F. Bakir, Z. Mazur Czerwiec, C. Sarraf and R. Rey, Numerical analysis of unsteady cavitating flow in an axial inducer, *Journal of Power and Energy*, 224 (A2) (2010) 223-238.

[10] Y. Tamura and Y. Matsumoto, Improvement of bubble model for cavitating flow simulations, *Journal of Hydrodynamics*, Ser. B, 21 (1) (2009) 41-46.

[11] Y. Yoshida, Y. Tsujimoto, D. Kataoka, H. Horiguchi and F. Wahl, Effects of alternate leading edge cutback on unsteady cavitation in 4-bladed inducers, *ASME J. Fluids Eng.,* 123 (4) (2001) 762-770.

[12] Y. Yoshida, M. Eguchi, T. Motomura, M. Uchiumi, H. Kure and Y. Maruta, Rotordynamic forces acting on three-bladed inducer under super synchronous/synchronous rotating cavitation, *ASME J. Fluids Eng.,* 132 (6) (2010) 061105.

[13] N. Tani, N. Yamanishi and Y. Tsujimoto, Influence of flow coefficient and flow structure on rotational cavitation in inducer, *ASME J. Fluids Eng.*, 134 (2) (2012) 706-714.

[14] H. Horiguchi, Y. Semenov, M. Nakano and Y. Tsujimoto, Linear stability analysis of the effects of camber and blade thickness on cavitation instabilities in inducer, *ASME J. Fluids Eng.*, 128 (3) (2006) 430-438.

[15] H. Horiguchi, S. Arai, J. Fukutomi, Y. Nakase and Y. Tsujimoto, Quasi-three-dimensional analysis of cavitation in an inducer, *ASME J. Fluids Eng.*, 126 (5) (2004) 709-715.

[16] T. Kimura, Y. Yoshida, T. Hashimoto and M. Shimagaki, Numerical simulation for vortex structure in a turbopump inducer: Close relationship with appearance of cavitation instabilities, *ASME J. Fluids Eng.*, 130 (5) (2008) 051104.

[17] S. S. Hong, D. J. Kim, J. S. Kim, C. H. Choi and J. Kim, Study on inducer and impeller of a centrifugal pump for a rocket engine turbopump, *Journal of Mechanical Engineering Science,* 227 (C2) (2013) 311-319.

[18] C. E. Brennen, A review of the dynamics of cavitating pumps, *Journal of Fluids Engineering-Transactions of the Asme*, 135 (6) (2013) 061301.

[19] X. W. Luo, W. Wei, B. Ji, Z. B. Pan, W. C. Zhou and H. Y. Xu, Comparison of cavitation prediction for a centrifugal pump with or without volute casing, *Journal of Mechanical Science and Technology*, 27(6) (2013) 1643-1648.

[20] S. Park and S. H. Rhee, Numerical analysis of the three-dimensional cloud cavitating flow around a twisted hydrofoil, *Fluid Dynamics Research*, 45 (1) (2013) 015502.

[21] H. L. Liu, J. Wang, Y. Wang, H. Zhang and H. Q. Huang, Influence of the empirical coefficients of cavitation model on predicting cavitating flow in the centrifugal pump, *International Journal of Naval Architecture and Ocean Engineering*, 6 (1) (2014) 119-131.

[22] B. Ji,, X. W. Luo, R. E. A. Arndt and Y. L. Wu, Numerical simulation of three dimensional cavitation shedding dynamics with special emphasis on cavitation-vortex interaction, *Ocean Eng*, 87 (2014) 64-77.

[23] B. Ji, X. W. Luo, Y. L. Wu, X. X. Peng and Y. L. Duan, Numerical analysis of unsteady cavitating turbulent flow and shedding horse-shoe vortex structure around a twisted hydrofoil, *International Journal of Multiphase Flow*, 51 (2013) 33-43.

[24] B. Ji, X. Luo, X. Wang, X. Peng, Y. Wu and H. Xu, Unsteady numerical simulation of cavitating turbulent flow around a highly skewed model marine propeller, *ASME J. Fluids Eng.*, 133 (1) (2011) 011102.

[25] R. Campos-Amezcua, S. Khelladi, Z. Mazur-Czerwiec, F. Bakir, A. Campos-Amezcua and R. Rey, Numerical analysis of unsteady cavitating flow in an axial inducer, *Journal of Power and Energy*, 227 (8) (2013) 858-868.

[26] D. A. Huang, Y. Q. Zhuang and R. Z. Cai, A computational method for cavitational flows based on energy conservation, *Journal of Mechanical Engineering Science*, 221 (11) (2007) 1333-1338.

[27] A. K. Singhal, M. M. Athavale, H. Y. Li and Y. Jiang, Mathematical basis and validation of the full cavitation model, *ASME J. Fluids Eng.*, 124 (3) (2002) 617-624.

XiaoMei Guo received her Ph.D. from Zhejiang Science and Technology University. Her research interests include multi-phase flow in fluid machinery, flow mechanism in high-speed pumps, and design optimization of fluid machines.

ZuChao Zhu is currently a professor and Ph.D. candidate supervisor in the Zhejiang Provincial Key Laboratory of Fluid Transmission Technology, Zhejiang Sci-Tech University, China. His main research interests include fluid machinery and engineering, and fluid power transmission and control.